UCRL- 96922
PREPRINT

Optical Spectroscopy of Cr^{3+} in ScF_3 and Sc_2O_3

G. Huber
Edward L. Ginzton Laboratory
Stanford University

Stephen A. Payne
L. L. Chase
William F. Krupke
Lawrence Livermore National Laboratory

This paper was prepared for submittal to
Journal of Luminescence

July 2, 1987

DISCLAIMER

Optical Spectroscopy of Cr^{3+} in ScF_3 and Sc_2O_3

G. Huber*

Edward L. Ginzton Laboratory

Stanford University

Stanford, California 94305 USA

Stephen A. Payne, L. L. Chase, and William F. Krupke**

Lawrence Livermore National Laboratory

University of California

Livermore, California 94550 USA

Abstract

We have obtained the absorption, excitation, and emission spectra, and the emission decay measurements for Cr^{3+} in the compounds ScF_3 and Sc_2O_3. Both of these materials have sixfold coordinated metal sites that are available for substitution by Cr^{3+}. From the analysis of the broadband spectra and the zero-phonon lines, we have derived information about the a_{1g}, e_g and the odd-parity, intensity-enabling coordinates. The quenching behavior of the Cr^{3+} luminescence is also explored. Finally, we discuss the effect of the next nearest neighbor cations on the crystal field splitting of Cr^{3+}

---

* On sabbatical leave from Institut für Angewandte Physik, Universität Hamburg, Jungiusstrasse 11, D-2000 Hamburg 36, Fed. Rep. Germany; work supported by Lawrence Livermore National Laboratory.

**Work performed under the auspices of the Division of Materials Sciences of the Office of Basic Energy Sciences, U.S. Department of Energy and the Lawrence Livermore National Laboratory under Contract No. W-7405-ENG-48.

1. Introduction

There has been a resurgence of interest in the Cr^{3+} ion, largely due to its utility as an impurity ion in solid state laser crystals. There are several properties intrinsic to the Cr^{3+} impurity which have proved to be valuable in the development of new solid state lasers. These include the efficient luminescence exhibited by Cr^{3+} in most materials, the special chemical stability of the trivalent oxidation state, and the three, broad, d-d absorption bands of Cr^{3+} which effectively couple the laser material to the flashlamp spectral output.

The tunability of Cr^{3+} is based upon the broad $^4T_2 \rightarrow {}^4A_2$ emission, which requires that the Cr^{3+} ion be situated in a "weak-field" crystal site. This condition is required because the excited state energy level ordering is sensitively dependent on the strength of the crystal field environment. In a strong field environment such as that present in Al_2O_3 (ruby), only the sharp $^2E \rightarrow {}^4A_2$ emission is observed,[1] while in $BeAl_2O_4$ (alexandrite), a mixture of the sharp $^2E \rightarrow {}^4A_2$ and broad $^4T_2 \rightarrow {}^4A_2$ emissions are present.[2,3] Current interests, however, are focusing exclusively on the vibronic $^4T_2 \rightarrow {}^4A_2$ emission, which predominates, for example, in the case of Cr^{3+} doped $Gd_3Sc_2Ga_3O_{12}$ (GSGG).[4,5] Other recently developed laser hosts which utilize low-field Cr^{3+} impurities as the active ions include $Gd_3Sc_2Al_3O_{12}$,[6] $SrAlF_5$,[7] $ZnWO_4$,[8] $ScBO_3$,[9] and $KZnF_3$.[10] The $^4T_2 \rightarrow {}^4A_2$ emission is also used to sensitize Nd^{3+} lasing action in several oxide garnets, such as GSGG.[11,12]

The question then arises as to what properties of the host crystal result in broadband Cr^{3+} emission. In general, Cr^{3+} is likely to see a weak field if it replaces a host metal ion with an ionic radius that is

similar to or larger than itself. If the difference in size between the Cr^{3+} ion and the cation for which it is substituted is too large, however, the possibility of nonradiative decay must be considered, because such conditions may allow for relatively strong excited state relaxation. The Sc^{3+} ion generally fulfills the "low-field" requirement, since the ionic radius of 0.75Å is slightly larger than the radius of 0.63Å for Cr^{3+}.

We have examined the properties of Cr^{3+} in two Sc-containing hosts, ScF_3 and Sc_2O_3. The metal sites of these crystals are octahedrally coordinated by the anions and therefore should readily incorporate the Cr^{3+} impurities into their lattice structure. Also, since Sc^{3+} and Cr^{3+} are both trivalent ions, there is no need for charge compensation. This attribute, in addition to the unitary nature of the compounds, serves to simplify the interpretation of their spectra.

In the case of ScF_3,[13] the six Sc-F distances are all 2.012Å, although the various octahedral bond angles are reported to vary from 87 to 93°. Thus, the Sc sites are coordinated by a slightly distorted octahedron of fluorines. The bixbyite crystal structure of Sc_2O_3,[14] on the other hand, has two types of distorted octahedral metal sites: one is trigonal and has inversion symmetry, and the other has C_{2V} point group symmetry and is, therefore, not centrosymmetric. The corresponding Sc-O distances are 2.120Å for the inversion site, while the C_{2V} site has distances of 2.080, 2.125 and 2.164Å for each of two Sc-O bonds. The presence of two sites may complicate the spectroscopy of this system. The Sc sites in ScF_3 and Sc_2O_3 are about 0.12Å larger than the Cr^{3+} ion. The ionic radius mismatch will tend to decrease the 3d-shell

crystal field splitting of the Cr^{3+} ion and red-shift the peak of the emission band.

In this work we report the absorption, emission and lifetime data of $ScF_3:Cr^{3+}$ and $Sc_2O_3:Cr^{3+}$. The spectroscopic methods and the crystal growth procedures are discussed in Section 2. The results and analyses are presented together in Sections 3A-D, where we consider the potential energy surfaces of the Cr^{3+} impurity in several coordinates, including the a_{1g}, e_g, and the odd-parity intensity-enabling modes. In Section 3E, the absorption and emission properties of Cr^{3+} in ScF_3 and Sc_2O_3 are compared with those of other compounds. Finally, in Section 4 we present our conclusions.

2. Experimental

A. Sample Preparation

The ScF_3 crystals were prepared by Herbert Newkirk at Lawrence Livermore National Laboratory from a flux comprised of a 20:80 mixture of ScF_3 and NaF, and approximately 1% doping of CrF_3. The mixture was heated in a platinum crucible from room temperature to 1100 C in 12 hours, and then slowly cooled to 700 C at about 3 C/hour. After rapid cooling back to room temperature, the single crystals of ScF_3 were leached from the flux with boiling water.

Single crystal fibers of Sc_2O_3:Cr were grown by the CO_2 laser-heated pedestal growth method.[15] The source material for growth was prepared by hot-pressing the powder into pellets, which were cut into bars with a 1 mm^2 cross-section. At a temperature of about 2400 C, single crystal fibers of high quality and 3 cm length could be pulled within 30 minutes. Details of the growth will be published elsewhere.[16]

B. Spectroscopic Measurements

The experimental techniques used were conventional in nature and therefore will be only briefly outlined. In all experiments, the sample temperature was varied between 12K and 300K with a closed-cycle helium refrigeration system, while a heating tape was used to raise the sample temperature above 300K. The absorption measurements were performed in the conventional manner using a computer-controlled Cary 17 spectrometer.

The excitation spectra were acquired by directing a continuous Xe lamp source through a computer-controlled monochromator and a 200 Hz chopper. The light output was focused onto the sample, and the resulting luminescence was separated from the exciting light with the appropriate color filters and then detected with a GaAs photomultiplier tube. Lock-in techniques were used to improve the signal-to-noise ratio. The combination of the lamp, color filters and monochromator was calibrated by replacing the sample with a silicon detector of known spectral response. The spectra were corrected so that the result was proportional to the number of luminescence photons divided by the number of incident photons.

The broadband emission spectra were obtained by exciting with either a Xe lamp or a helium-neon laser, and by monitoring the luminescence with a PbS detector. The monochromator-detector combination was calibrated using a tungsten-halogen lamp of known spectral output. The spectra were corrected to be in units of photons/second per unit energy interval. The emission fine-structure was resolved in a separate experiment in which the sample was excited by either a helium-neon laser or the second harmonic of a YAG laser, and the luminescence was recorded by dispersing the spectrum onto the array of a reticon detector (PAR 1420).

The emission lifetime measurements were obtained by exciting the sample with an N_2 laser at 337 nm and detecting the emission with a GaAs photomultiplier tube. A few measurements involved pumping with a dye laser. The emission decays were recorded with either a computer-controlled transient digitizer, or by photon counting, using a multichannel analyzer.

3. Results and Analysis

A. Absorption and Emission Spectra

The absorption (excitation) and emission spectra of Cr^{3+} in ScF_3 and Sc_2O_3 appear in Fig. 1. Since the ScF_3 samples were rather small (2 X 1 X 1 mm^3), three crystals were arranged in an array to obtain the absorption spectrum in Fig. 1. The Sc_2O_3 samples, on the other hand, were thin fibers and therefore required that excitation rather than absorption spectra be taken. The $^4A_2 \rightarrow {}^4T_2$ absorption of Cr^{3+} occurs at 14,280 cm^{-1} and 15,200 cm^{-1} for ScF_3 and Sc_2O_3, respectively, at 14K. From the $3d^3$ Tanabe-Sugano diagram, the peak of the $^4A_2 \rightarrow {}^4T_2$ transition is known to occur at the energy 10Dq,[17] so that the corresponding Dq values for these materials are 1428 and 1520 cm^{-1}. The ratio of these Dq parameters for the oxide and fluoride is 1.06, while from simple electrostatic considerations,[18] we can predict this ratio to be 1.57 by using the Sc-anion distances of the pure hosts and taking the ratio of the O and F charges to be 2. Thus, as is often the case, it is only possible to predict the qualitative nature of a trend with simple crystal field theory.

The second band in Fig. 1, which could not be fully resolved for Sc_2O_3, is due to the $^4A_2 \rightarrow {}^4T_1a$ transition. This band peaks at a rather low energy for Sc_2O_3 compared with predictions of a cubic crystal field model. This result may be due to a splitting of the ^4T_1a state by the low symmetry field present at the Sc^{3+} site. The $^4A_2 \rightarrow {}^4T_1a$ transition is observed to occur at 21,800 cm^{-1} for $ScF_3:Cr^{3+}$, and the Fano antiresonance[19] due to the $^4A_2 \rightarrow {}^2E$ transition is observed as a dip near 15,200 cm^{-1}.

The emission spectra in Fig. 1 are due to the $^4T_2 \rightarrow {}^4A_2$ transition. The emission spectra of $Sc_2O_3:Cr^{3+}$ peak at nearly the same energy at 14K and 295K. Since the width increases with increasing temperature, we can estimate the effective symmetric mode frequency, $\hbar\omega$, with the well-known result[20]

$$\sigma(T)^2 = \sigma(0)^2 \coth \frac{\hbar\omega}{2kT} \qquad (1)$$

where $\sigma(T)$ is the width of the band at temperature T and k is Boltzmann's constant. Using the data in Fig. 1, along with spectra at other temperatures, we find that the effective symmetric mode frequency is $\hbar\omega = 340\pm50$ cm^{-1}. Using the same procedure for $ScF_3:Cr^{3+}$, we get $\hbar\omega = 205\pm20$ cm^{-1}. The Dq and $\hbar\omega$ values, as well as the full-width-at-half-maxima (FWHM), are listed in Table 1. The FWHM for the absorption and emission bands of $Sc_2O_3:Cr^{3+}$ are the same within experimental error, as is most often the case. The data for ScF_3 is, however, somewhat surprising. Firstly, the FWHM for the absorption and emission bands differ substantially from each other, and, secondly, the emission peak is observed to shift with temperature. These aspects of ScF_3 will be considered further in Section 3C.

B. Zero-Phonon Lines (ZPL)

The structure near the origin of the emission spectra is displayed in Fig. 2. The understanding of the ZPL's for $ScF_3:Cr^{3+}$ is straightforward and will be discussed first. The $^4T_2$ excited state is expected to have four spin-orbit components since S=3/2 transforms as the U' representation in the O_h double group and $U' \times T_2 = E' + E'' + 2U'$. There is, however, an additional factor that must be taken into account, which involves the influence of the Jahn-Teller effect on the magnitude of the spin-orbit splitting (known as the Ham effect). These calculations have been performed by Güdel and Snellgrove,[21] who in turn followed the treatment of Sturge.[22] Using their calculations, we find that with $3E_{JT}/\hbar\omega_e = 2.2$ the observed peak positions can be reasonably well reproduced, see Table 2. Here, E_{JT} is the Jahn-Teller energy and $\hbar\omega_e$ is the frequency of the e_g mode. Our value of $3E_{JT}/\hbar\omega_e$ is somewhat smaller than the fits that Knochenmuss, et.al., obtained for the $Cs_2NaInCl_6:Cr^{3+}$ and $Cs_2NaYCl_6:Cr^{3+}$ systems.[23] Now that the levels have been assigned and the degeneracies, g, are known, we can predict the relative intensity of the lines due to states i=U',U' and E' compared to the E'' state, with the relationship

$$\frac{I(i)}{I(E'')} = \frac{g(i)}{g(E'')} \exp\left(\frac{-(E(i)-E(E''))}{kT}\right) \qquad (2)$$

Using T=12K, the predicted intensity ratios compare favorably with those measured, see Table 2. The intensity calculations assume that the transition rates from each of the 2+4+4+2=12 spin-orbit components are the same, as is expected. It is worthwhile to note that these spin-orbit assignments also provide good evidence that Cr^{3+} is situated in a nearly

perfect octahedral environment in ScF_3, since a lower symmetry would result in additional splitting of the origin lines. If we assume that the e_g frequency is nearly the same as the a_{1g} frequency (as determined below in Section 3C), we find that $E_{JT} = 280\ cm^{-1}$ for $ScF_3:Cr^{3+}$.

We considered the possibility that the two lines observed in Fig. 2 for $Sc_2O_3:Cr^{3+}$ might be due to the presence of multiple Cr^{3+} sites. We found, however, that the spectra of two samples from different growth runs were very similar. In addition, we time-resolved the emission by using a pulsed excitation source and observed that the two lines exhibit the same emission lifetime. Therefore we conclude that the lines displayed in Fig. 2 are due to a single Cr^{3+} site. We also note that the background rising to higher energy is not due to Cr^{3+}, but is probably due to some other impurity.

The interpretation of the ZPL structure for Sc_2O_3 is much more complicated than for ScF_3, because the sites of Sc_2O_3 are distorted from exact octahedral symmetry. The lines observed in Fig. 2 therefore result from a combination of spin-orbit and crystal-field splitting, as well as the Jahn-Teller effect. The intensity ratio of the two lines in Fig. 2 is larger than that expected from the 33 cm^{-1} separation if it is assumed that they are purely spin-orbit split components, which shows that the upper level must have a much greater transition probability than the lower level. This is an indication that the low symmetry crystal field is playing an important role in the observed splitting and the transition probabilities of the individual lines.

C. Analysis of the Emission Line Shapes

The emission lineshapes for Cr^{3+} doped ScF_3 and Sc_2O_3 at 14K have been reproduced in Fig. 3. The position of the ZPL can be used to fit the broad emission band to the Pekarian form for T=0K with[24]

$$W_p = (S^p \exp(-S))/p! \qquad (3)$$

where p is the number of emitted phonons and S is the Huang-Rhys factor. A more detailed formula was actually used to take the finite temperature into account.[25,26] We see in the upper frame that we have obtained a good fit to the experimental data using S=3.0 and $\hbar\omega$=380 cm^{-1} for ScF_3. This value of 380 cm^{-1} for the fully symmetric vibrational frequency is quite different from the $\hbar\omega$=205 cm^{-1} result obtained by analyzing the temperature dependence of the emission bandwidth, (see Table 3 and Section 3A). It is possible, however, that the use of Eq. 1 is not valid since this theory also predicts that the emission band peak should not shift strongly with changing temperature. This suggests that the anharmonicity of the excited and ground potential energy surfaces may be significant for the Cr^{3+} ion in ScF_3. Anharmonicity could be responsible for the shift of the emission band peak and also for the anomalously large increase in the emission bandwidth as the temperature is increased. The effects of anharmonicity have been previously considered for the case of $KMgF_3:Co^{2+}$.[27]

We were not able to achieve a line shape fit of comparable quality for $Sc_2O_3:Cr^{3+}$, as shown in the lower frame of Fig. 3. The calculated points are the result of fitting the high energy side of the spectrum. To test whether the discrepancy was due to the presence of multiple sites, we measured the emission lifetime at two energies, as

shown in Fig. 4. When exciting at 19,460 cm^{-1}, a single exponential decay of 91 μs was obtained by detecting the light at 11,760 cm^{-1}, while a double exponential consisting of the lifetimes 86 μs and 373 μs results from monitoring at 9,090 cm^{-1}. This indicates the existence of a second site, which has a longer lifetime and is red-shifted relative to the other site. This may also mean that the fit with S=4.5 and $\hbar\omega$= 410 cm^{-1} is more likely to be a representation of the parameters that characterize the 91 μs site. The vibrational frequency of 410 cm^{-1} is also similar to the value of 340 cm^{-1} derived from the use of Eq. 1. As mentioned in Section 1, there are two Sc^{3+} sites in Sc_2O_3; one is centrosymmetric and the other is not.[14] We can speculate at this point that the inversion site might have the 373 μs lifetime and the more distorted site has a larger induced dipole moment and therefore a shorter lifetime of 91 μs. With the information currently available, it appears that both S and $\hbar\omega$ are larger for the oxide compared to the fluoride.

D. Emission Lifetime Results

The emission lifetime results are displayed in Fig. 5. All of the decays observed for $ScF_3:Cr^{3+}$ could be described with a single exponential function. This is reasonable since there is only one kind of metal site in the ScF_3 lattice and no charge compensation is required.

The decay times change substantially as a function of temperature for $ScF_3:Cr^{3+}$. We have fitted the emission lifetimes of $ScF_3:Cr^{3+}$ in Fig. 5 to the equation[20]

$$\frac{1}{\tau} = \frac{1}{\tau_0} \coth\left(\frac{\hbar\omega}{2kT}\right) \qquad (4)$$

where τ_o=920 μs and $\hbar\omega$=167 cm^{-1} is the frequency of the intensity-enabling vibration in the excited state. Thus these results show that the transition strength of the parity-forbidden $^4T_2 \rightarrow {}^4A_2$ transition is being induced by an effective odd-parity vibration with a frequency of 167 cm^{-1}. This predominance of vibrationally induced transitions is consistent with the presence of a nearly perfect octahedron of fluorines implied by the spin-orbit analysis of Section 3B. The fit in Fig. 5 also indicates that there is no indication of quenching up to temperatures of 450K.

The increase in the absorption strength of $ScF_3:Cr^{3+}$ with rising temperature is not as dramatic as observed for the emission rates, as seen in Fig. 1. The enabling frequency derived by fitting the increase in absorption strength is therefore much higher, being 400±50 cm^{-1}. It therefore appears that the enabling mode frequencies of the ground and excited states differ substantially in this particular coordinate. A similar situation occurred in the case of the fully symmetric coordinate, however, as evidenced by the large difference in the low temperature energetic separations of the ZPL from the emission and absorption peaks, which are 790 and 1240 cm^{-1}, respectively.

The lifetimes of Cr^{3+} in Sc_2O_3 are plotted in the lower frame. The low temperature lifetime is a factor of 6.6 faster than that of ScF_3. This is due to the noncentrosymmetric nature of the site in Sc_2O_3.

The decays reported in Fig. 5 were nonexponential in form, probably because the energy of 29,670 cm^{-1} (337 nm) used to acquire this data did not overlap the peak of an absorption band, as did the wavelength

utilized for the data in Fig. 4, and both Cr^{3+} sites were observed. Additional decay measurements resulting from excitation at 16300 cm^{-1} produced lifetimes about 20% higher than those plotted in Fig. 5. We can see that the square point at 295K in Fig. 5, which was obtained from Fig. 4, is nevertheless in reasonable agreement with the average lifetimes derived from 337 nm excitation.

It is clear from Fig. 5 that the lifetimes are significantly reduced at temperatures above 300K. This is almost certainly due to competition from nonradiative decay. We can qualitatively understand that the nonradiative decay occurs at lower temperature for Sc_2O_3 compared to ScF_3 because the values of S and $\hbar\omega$ are larger for this system. The activation energy derived from the data in Fig. 5 is roughly E_A=3500 ± 1000 cm^{-1}, depending on the choice of the frequency factor. This contrasts sharply with the value of E_A=18,000 cm^{-1} determined by using S=4.5 and $\hbar\omega$=410 cm^{-1} from Fig. 3 to calculate the cross-over point of the ground and excited state potential energy surfaces (within the harmonic approximation) with

$$E_A = \frac{(E_{ZPL} - S\hbar\omega)^2}{4S\hbar\omega} \qquad (5)$$

In addition, detailed calculations using the equations of Struck and Fonger[25,26] show that the single configurational coordinate model substantially underestimates the nonradiative decay rate. This underestimation from the analysis of the spectra has been noted by other workers.[27-29] Again, it is possible that anharmonicity may play an important role since the nonradiative decay paths usually involve displacements far from the equilibrium configuration.[27]

E. Comparison with the Cr^{3+} Spectra of Other Compounds

The Cr^{3+} Dq parameters along with the metal-anion separations of several compounds are listed in Table 4. It appears that, despite the similar Sc-F separations of K_2NaScF_6 and ScF_3,[13,30] the crystal field splitting of 1560 cm^{-1} in the elpasolite[28] is a good deal larger than the 1410 cm^{-1} splitting in ScF_3, respectively. Since we know that the Sc^{3+} ionic radius is about .12Å larger than that of Cr^{3+}, the first tendency might be to attribute the difference in Dq to dissimilar lattice relaxation at the impurity site. This possibility arises because of the expected inverse fifth-power dependence (and hence sensitivity) of Dq on the Cr-F separation. To test this theory, we can compare the Dq's of the pure compounds K_2NaCrF_6 and CrF_3, where the exact Cr-F distances are known,[30,31] as is summarized in Table 4. We note, however, that despite the similar Cr-F separation of these materials, the elpasolite again has a considerably larger Dq value. Wood, et.al.,[32] have suggested some time ago that the larger Dq of K_2NaCrF_6 compared to CrF_3 can be attributed to the effect of the next nearest neighbor (n.n.n.) metal ion upon the fluorines that directly surround the Cr^{3+} ion. In the case of the elpasolite, the n.n.n. is Na^+ compared to Cr^{3+} for CrF_3 (Sc^{3+} for ScF_3). It is possible that the neighboring trivalent cations, Cr^{3+} or Sc^{3+}, reduce the effective charge of the fluorines that surround Cr^{3+} more so than the monovalent n.n.n. Na^+ ions of the elpasolite structure. Thus, the more recent data obtained for Cr^{3+}-doped K_2NaScF_6 and ScF_3 supports the original theory of Wood, et.al.[32]

From the data in Table 4, it is apparent that the effect of the larger Sc^{3+} site on the Cr^{3+} spectra is not as important as might be expected. This might be due to the relaxation of the fluorines of the impurity site, which leads to the existence of similar Cr^{3+} sites in K_2NaCrF_6 and K_2NaScF_6:Cr^{3+} (and in CrF_3 and ScF_3:Cr^{3+}).
A dramatic manifestation of lattice relaxation about the Cr^{3+} ion was observed in Cr^{3+}-doped CdF_2, CaF_2, SrF_2 and BaF_2, where the environment is found to change from eight- to sixfold coordination when the alkaline earth ion is replaced by Cr^{3+}.(33)

The interpretation espoused above is supported by the data for the Cr^{3+}-doped oxide garnets shown in Table 5. Cr^{3+} is known to substitute for the octahedrally coordinated Sc^{3+} ion in the $Gd_3Sc_2Ga_3O_{12}$ (GSGG) host. We see that the substitution of the Sc^{3+} ion by Ga^{3+} has a similar effect on Dq as does replacing Gd^{3+} with Y^{3+}, or the tetrahedral Ga^{3+} ion with Al^{3+}.(4,5) This suggests that the effect due to the size of the substitutional site into which Cr^{3+} is incorporated is comparable to the indirect influence of the other cations on the oxygens that coordinate Cr^{3+}. This is reasonable since the wavefunction of the oxygen ion is expected to be very sensitive to the local environment in which it is situated.(34)

4. Conclusions

The conclusions concerning the spectral properties of Cr^{3+} in ScF_3 and Sc_2O_3 are summarized below:

1. The Dq value is slightly larger in Sc_2O_3 compared to ScF_3, being 1520 versus 1428 cm^{-1}. This increase is much less than that

predicted from crystal field theory. The ScF_3 and Sc_2O_3 hosts have the lowest crystal fields of all known Sc-compounds. The rather low Dq values of these materials can in part be attributed to the larger ionic radius of Sc^{3+} compared to Cr^{3+}, but also to the next-nearest-neighbor interaction of the Sc^{3+} ions with the oxygens or fluorines that are coordinated to the Cr^{3+} impurity.

2. From the analysis of the emission lineshape and the position of the ZPL's, we found that S=3.0 and $\hbar\omega$=380 cm^{-1} for ScF_3; the corresponding values for Sc_2O_3 are 4.5 an 410 cm^{-1}. Some uncertainty remains concerning the Sc_2O_3 data because of the existence of two inequivalent sites.
3. The energetic separations of the ZPL from the emission and absorption peaks are 790 and 1240 cm^{-1}, respectively, for $ScF_3:Cr^{3+}$, while the values are 1630 and 1770 cm^{-1} for Sc_2O_3. This shows that the ground and excited state potential energy surfaces are substantially different from each other for $ScF_3:Cr^{3+}$.
4. The oscillator strength of the parity-forbidden $^4T_2$-$^4A_2$ ($3d^3$-$3d^3$) transition is induced by different mechanisms for these crystals. For the case of Sc_2O_3, the static, odd-parity component of the crystal field provides electric dipole oscillator strength for the transition. The $ScF_3:Cr^{3+}$ system, on the other hand, acquires oscillator strength via a dynamical mixing process.
5. The structure of the spin-orbit components of the $^4T_2$ excited state for $ScF_3:Cr^{3+}$ has been analyzed to derive a Jahn-Teller energy of about 280 cm^{-1}. On the other hand, the zero-phonon lines of $Sc_2O_3:Cr^{3+}$ are found to be influenced by the low symmetry of the crystal field present at the Sc^{3+} site.

6. Emission quenching was not observed up to the temperature of 450K for $ScF_3:Cr^{3+}$, while nonradiative decay begins to become significant in $Sc_2O_3:Cr^{3+}$ near 300K. This is qualitatively consistent with the larger value of the $S\hbar\omega$ product for Sc_2O_3.

Acknowledgements

We wish to thank Prof. Robert Byer for accommodating one of us (G. Huber) during his sabbatical stay at Stanford University, and also R. S. Feigelson and R. K. Route, who made the growth of the Sc_2O_3 samples possible. We are grateful to Herbert Newkirk at Lawrence Livermore National Laboratory for providing the $ScF_3:Cr^{3+}$ samples, and also to John Caird, who suggested that this material might be an interesting host.

References

1. O. Deutschbein, Am. d. Phys 14 (1932) 712, 729; ibid. 20 (1934) 828.

2. M. L. Shand and J. C. Walling, IEEE J. Quant. Electron. 18 (1982) 1152; M. L. Shand and H. P. Jenssen, IEEE J. Quant. Electron. 19 (1983) 480.

3. R. C. Powell, L. Xi, X. Gang, and G. J. Quarles, Phys. Rev. B 32 (1985) 2388.

4. B. Struve and G. Huber, J. Appl. Phys. 57 (1985) 45.

5. B. Struve and G. Huber, Appl. Phys. B 36 (1985) 195.

6. J. V. Meier, N. P. Barnes, D. K. Remelius and M. R. Kokta, IEEE J. Quantum Electron. 22 (1986) 2058; J. Drube, B. Struve and G. Huber, Opt. Commun. 50 (1984) 45.

7. H. P. Jenssen and S. T. Lai, J. Opt. Soc. Am. B 3 (1986) 115.

8. W. Kolbe, K. Petermann, and G. Huber, IEEE J. Quantum Electron. 21 (1985) 1596.

9. S. T. Lai, B. H. T. Chai, M. Long and R. C. Morris, IEEE Quantum Electron. 22 (1986) 1931.

10. U. Brauch and U. Durr, Opt. Commun. 49 (1984) 61.

11. W. F. Krupke, M. D. Shinn, J. E. Marion, J. A. Caird and S. E. Stokowski, J. Opt. Soc. Am. B 3 (1986) 102.

12. E. V. Zharikov, N. N. Il'ichev, V. V. Laptev, A. A. Malyutin, V. G. Ostroumov, P. P. Pashinin, A. S. Pimenov, V. A. Smirnov and I. A. Shcherbakov, Sov. J. Quantum Electron. 13 (1983) 82; V. G. Ostroumov, Y. S. Privis, V. A. Smirnov, and I. A. Shcherbakov, J. Opt. Soc. Am. B 3 (1986) 81; A. L. Denisov, V. G. Ostroumov, Z. S. Saidov, V. A. Smirnov, and I. A. Shcherbakov, J. Opt. Soc. Am. B 3 (1986) 95.

13. E. G. Ippolitov and A. G. Maklachkov, Russion J Inorg. Chem. 15 (1970) 753; W. Nowacki, Zeitschr. f. Kristallographie 101 (1939) 273; L. Lösch, Ch. Hebecker, and Z. Ranft, Z. Anorg. Allg. Chem. 491 (1982) 199.

14. R. Norrestam, Arkiv for Kemi 29 (1967) 343.

15. R. S. Feigelson, J. Cryst. Growth 79 (1986) 669.

16. G. Huber, R. S. Feigelson and R. K. Route, J. Cryst. Growth, to be published.

17. Y. Tanabe and S. Sugano, J. Phys. Soc. Japan 9 (1954) 753, 766.

18. J. S. Griffith, The Theory of Transition Metal Ions (University Press, Cambridge, 1971).

19. M. D. Sturge, H. J. Guggenheim, and M. H. L. Pryce, Phys. Rev. B 2 (1970) 2459.

20. A. M. Stoneham, Theory of Defects in Solids (Clarendon Press, Oxford, 1975).

21. H. U. Güdel and T. R. Snellgrove, Inorg. Chem. 17 (1978) 1617.

22. M. D. Sturge, Phys. Rev. B 1 (1970) 1005.

23. R. Knochenmuss, C. Reber, M. V. Rajasekharan, and H. U. Güdel, J. Chem. Phys 85 (1986) 4280.

24. M. H. L. Pryce in Phonons, ed. R. W. H. Stevenson (Oliver and Boyd, Edinburgh, 1966).

25. P. Albers, E. Stark, and G. Huber, J. Opt. Soc. Am. B 3 (1986) 134.

26. C. W. Struck and W. H. Fonger, J. Luminesc. 10 (1975) 1; ibid., 18/19, (1979), 101.

27. M. D. Sturge, Phys Rev. B 8 (1973) 6.

28. L. J. Andrews, A. Lempicki, B. C. McCollum and C. J. Giunta, Phys. Rev. B 34 (1986) 2735.

29. R. H. Bartram, J. C. Charpie, L. J. Andrews, and A. Lempicki, Phys. Rev. B 34 (1986) 2741.

30. V. S. Scheider and R. Hoppe, Zeitschr. Anorg. Allgemeine Chemie 376 (1970) 268.

31. K. Knox, Acta Cryst. 13 (1960) 507.

32. D. L. Wood, J. Ferguson, K. Knox and J. F. Dillion, Jr., J. Chem. Phys. 39 (1963) 890.

33. S. A. Payne, L. L. Chase, and W. F. Krupke, J. Chem. Phys. 86 (1987) 3455.

34. J. R. Tessman, A. H. Kahn, and W. Shockley, Phys. Rev. 92 (1953) 890.

Figure Captions

1. Absorption or excitation and low-resolution emission spectra of $ScF_3:Cr^{3+}$ and $Sc_2O_3:Cr^{3+}$ at 295K and 14K. The spectra of both systems are indicative of fairly weak crystal field splitting.

2. Emission spectra in the vicinity of the origin for $ScF_3:Cr^{3+}$ and $Sc_2O_3:Cr^{3+}$ at 12K and 50K. The background observed for $Sc_2O_3:Cr^{3+}$ is not due to Cr^{3+}. The fine-structure of $ScF_3:Cr^{3+}$ is due to the Ham reduction of the spin-orbit split components. The interpretation for Sc_2O_3 is complicated by the presence of a low symmetry crystal field.

3. Pekarian fits to the emission line shapes of $ScF_3:Cr^{3+}$ and $Sc_2O_3:Cr^{3+}$ at 14K using the parameters shown. The $S \cdot h\omega$ product is larger for the oxide compared to the fluoride.

4. Emission decays for $Sc_2O_3:Cr^{3+}$ at room temperature resulting from exciting at 19,460 cm^{-1}. A single exponential decay of 91 μs is observed at 11,760 cm^{-1}, while two decays with lifetimes of 86 μs and 373 μs are resolved at 9,090 cm^{-1}, indicating the presence of a second site.

5. Emission lifetime measurements for $ScF_3:Cr^{3+}$ and $Sc_2O_3:Cr^{3+}$ as a function of temperature. The slow decrease in the lifetime for ScF_3 is due to the dynamical increase of the oscillator strength for the $^4T_2 \rightarrow {}^4A_2$ transition, while the change for $Sc_2O_3:Cr^{3+}$ above 300K is due to nonradiative decay.

Table 1

Properties of the $^4T_2$-$^4A_2$ transition of Cr^{3+}
(energies are given in cm^{-1})

Crystal	Dq (14K)	Full-Width at Half-Maximum (14K)		Symmetric Mode (emission width vs. temp.)
		Absorption	Emission	
ScF_3	1428	2130±200	1570	205±20
Sc_2O_3	1520	2070	2340	340±50

Table 2.

Zero-phonon lines of $ScF_3:Cr^{3+}$ at 12K

	Energy (cm^{-1})		Intensity	
Representation	Measured	Calculated	Measured	Calculated
E''	0	(0)	1.00	(1.00)
U'	14	17	0.31	0.37
U'	36	33	0.04	0.03
E'	-	47	0.00	0.00

Table 3

Determination of symmetric mode frequency of Cr^{3+} from the emission spectra

(energies are given in cm^{-1})

Crystal	Method I, T-dependence	Method II, Line shape analysis
ScF_3	205±20	380 (S=3.0)
Sc_2O_3	340±50	410 (S=4.5)

Table 4

Comparison of Sc-containing crystals with pure Cr^{3+} compounds (300K)

Crystal	Dq (cm^{-1})	metal-anion distance (Å)
K_2NaCrF_6	1610[a]	1.93[b]
$K_2NaScF_6:Cr^{3+}$	1560[c]	1.99[b]
CrF_3	1460[a]	1.90[d]
$ScF_3:Cr^{3+}$	1410	2.01[e]

(a) Ref. 32
(b) Ref. 30
(c) Ref. 28
(d) Ref. 31
(e) Ref. 13

Table 5

Comparison of Cr^{3+}-doped garnets (300K)

Crystal	Dq (cm^{-1})	Change relative to GSGG
$Gd_3Sc_2Ga_3O_{12}$ (GSGG)	1563[a]	• • •
$Y_3Sc_2Ga_3O_{12}$ (YSGG)	1613[a]	Gd→Y, +50 cm^{-1}
$Gd_3Ga_2Ga_3O_{12}$ (GGG)	1597[a]	Sc→Ga, +34 cm^{-1}
$Gd_3Sc_2Al_3O_{12}$ (GSAG)	1587[b]	Ga→Al, +24 cm^{-1}

(a) Ref. 5

(b) Ref. 4

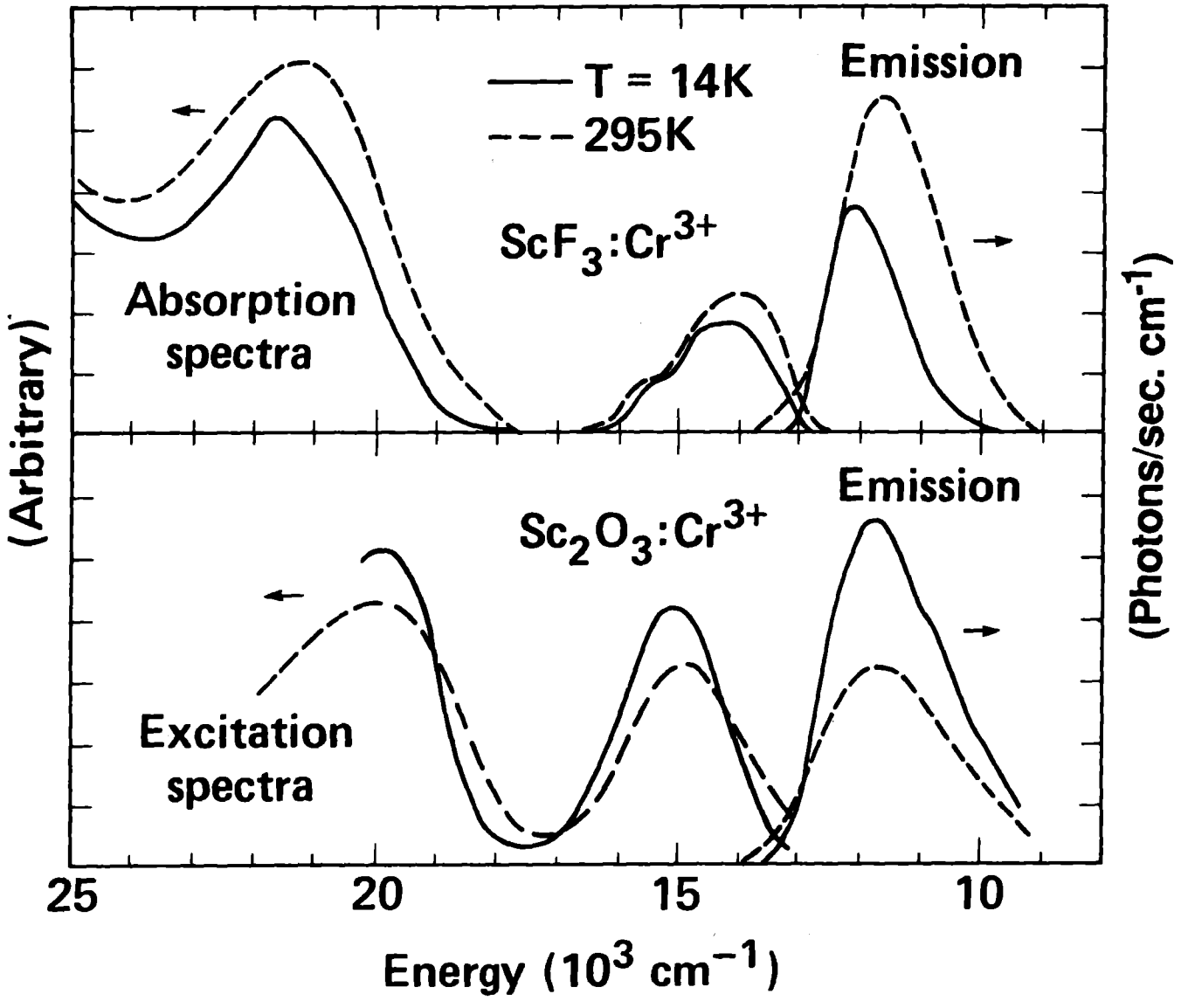
T = 14K
295K
Emission
$ScF_3:Cr^{3+}$
Absorption spectra
(Arbitrary)
Emission
$Sc_2O_3:Cr^{3+}$
Excitation spectra
(Photons/sec. cm^{-1})
25
20
15
10
Energy (10^3 cm^{-1})

Figure 1

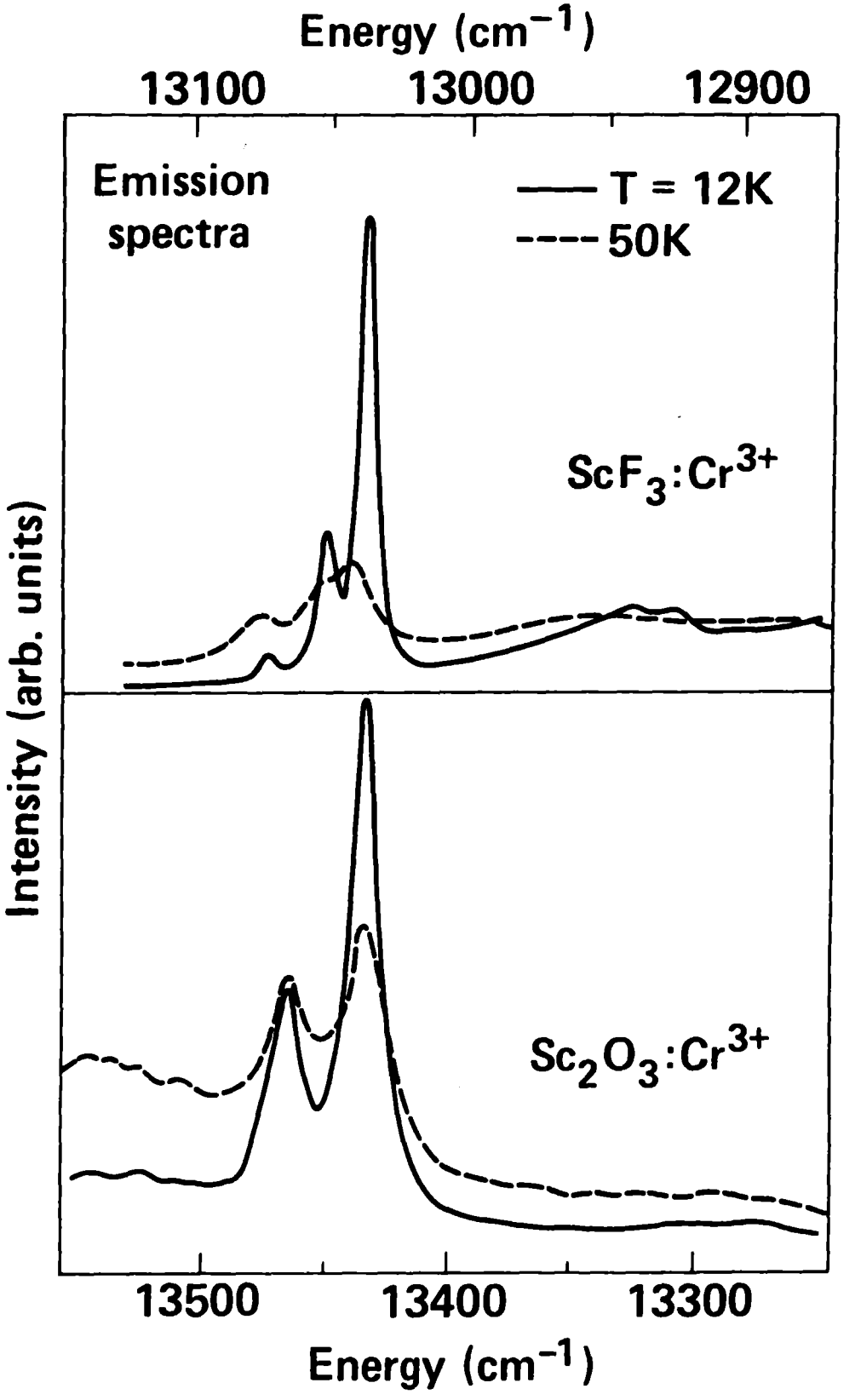

Figure 2

70-00-0387-0514A

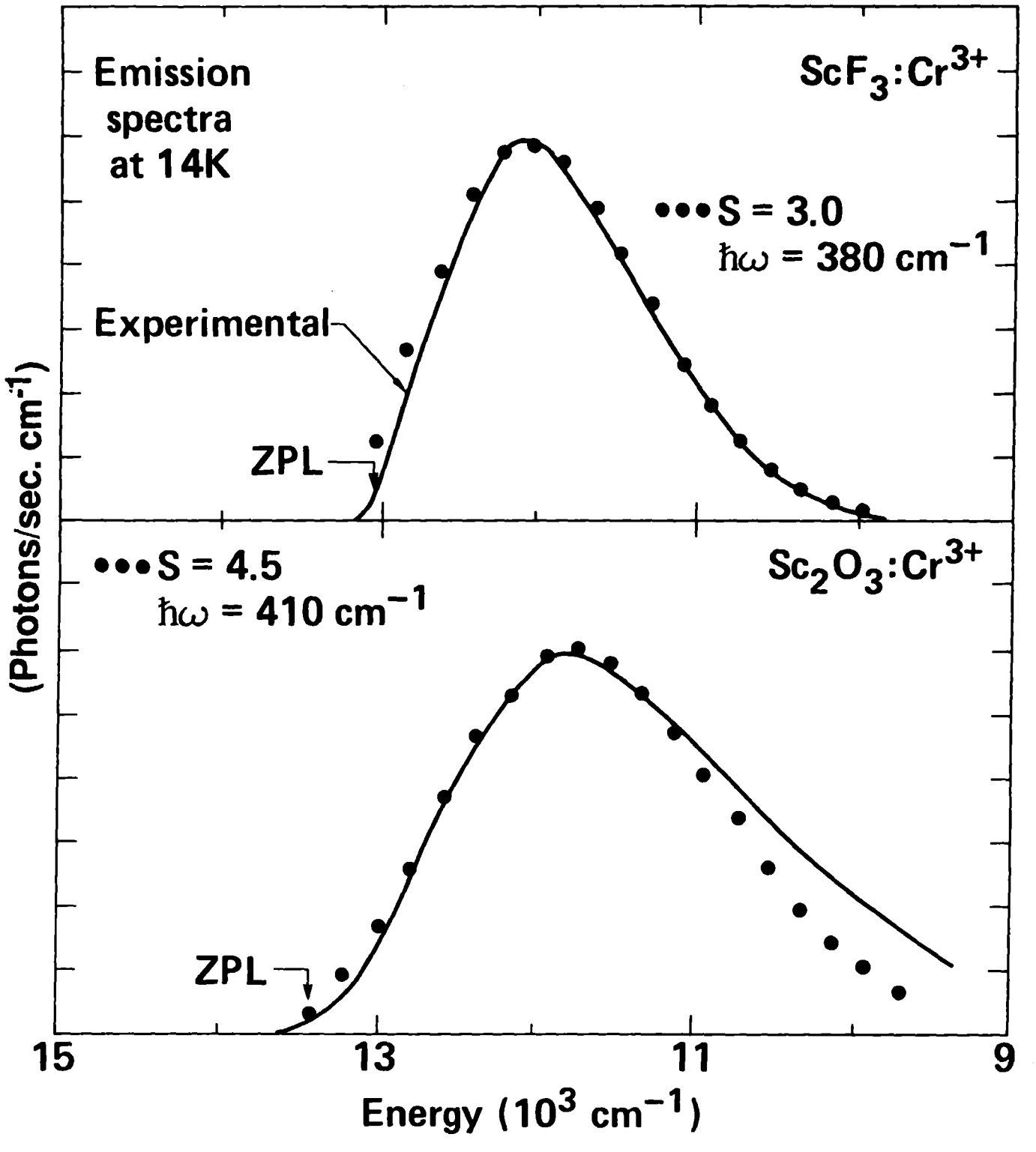
Emission
spectra
at 14K
$ScF_3:Cr^{3+}$
•••S = 3.0
$\hbar\omega = 380\ cm^{-1}$
Experimental
ZPL
(Photons/sec. cm^{-1})
•••S = 4.5
$\hbar\omega = 410\ cm^{-1}$
$Sc_2O_3:Cr^{3+}$
ZPL
15
13
11
9
Energy ($10^3\ cm^{-1}$)

Figure 3

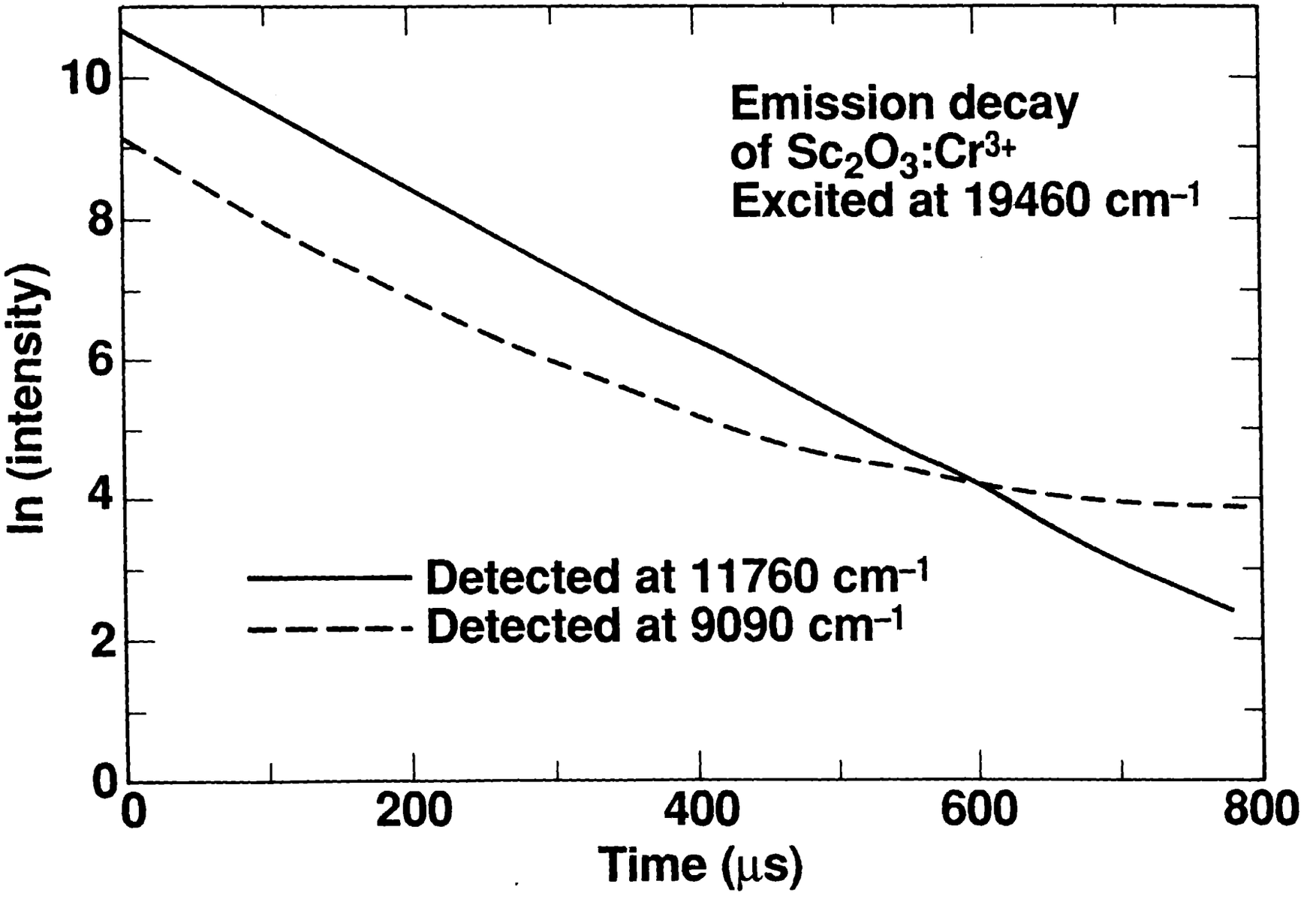

70-00-0387-0584

Figure 4

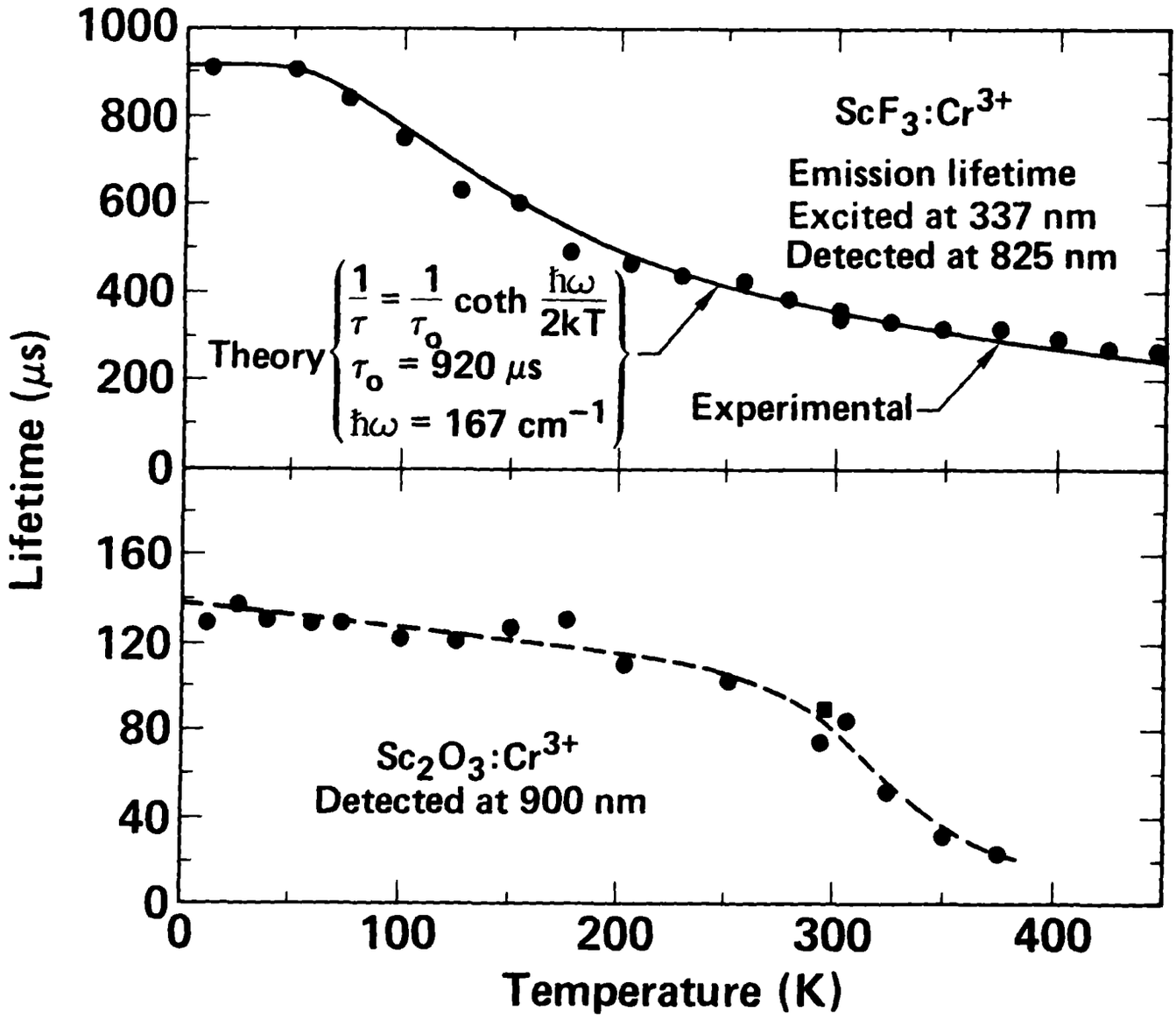
1000
800
600
400
200
0
160
120
80
40
0
Lifetime (μs)
ScF3:Cr3+
Emission lifetime
Excited at 337 nm
Detected at 825 nm
Theory
1/τ = 1/τo coth ħω/2kT
τo = 920 μs
ħω = 167 cm−1
Experimental
Sc2O3:Cr3+
Detected at 900 nm
0
100
200
300
400
Temperature (K)

Figure 5